Matter and Radiation at Extremes

Bright betatron radiation from direct-laser-accelerated electrons at moderate relativistic laser intensity

Cite as: Matter Radiat. Extremes **6**, 048401 (2021); https://doi.org/10.1063/5.0042315
Submitted: 29 December 2020 • Accepted: 25 May 2021 • Published Online: 09 July 2021

O. N. Rosmej, X. F. Shen, A. Pukhov, et al.

Matter and Radiation at Extremes | RESEARCH ARTICLE | scitation.org/journal/mre

Bright betatron radiation from direct-laser-accelerated electrons at moderate relativistic laser intensity

Cite as: Matter Radiat. Extremes 6, 048401 (2021); doi: 10.1063/5.0042315
Submitted: 29 December 2020 • Accepted: 25 May 2021 •
Published Online: 9 July 2021

O. N. Rosmej,[1,2,3,a)] X. F. Shen,[4] A. Pukhov,[4] L. Antonelli,[5] F. Barbato,[6] M. Gyrdymov,[2] M. M. Günther,[1] S. Zähter,[1] V. S. Popov,[7,8] N. G. Borisenko,[9] and N. E. Andreev[7,8]

AFFILIATIONS

[1]GSI Helmholtzzentrum für Schwerionenforschung GmbH, Planckstraße 1, 64291 Darmstadt, Germany
[2]Goethe University, Frankfurt, Max-von-Laue-Straße 1, 60438 Frankfurt am Main, Germany
[3]Helmholtz Forschungsakademie Hessen für FAIR (HFHF), Campus Frankfurt am Main, Max-von-Laue-Straße 12, 60438 Frankfurt am Main, Germany
[4]Heinrich-Heine-University Düsseldorf, Universitätsstraße 1, Düsseldorf, Germany
[5]York Plasma Institute, University of York, Church Lane, Heslington, York YO10 5DQ, United Kingdom
[6]University of Bordeaux, CNRS, CEA, CELIA, UMR 5107, F-33405 Talence, France
[7]Joint Institute for High Temperatures, RAS, Izhorskaya St. 13, Bldg. 2, 125412 Moscow, Russia
[8]Moscow Institute of Physics and Technology (State University), Institutskiy Pereulok 9, 141700 Dolgoprudny, Moscow Region, Russia
[9]P. N. Lebedev Physical Institute, RAS, Leninsky Prospekt 53, 119991 Moscow, Russia

Note: This paper is part of the Special Issue on Matter in extreme states created by laser.

[a)]**Author to whom correspondence should be addressed:** o.rosmej@gsi.de.
Permanent address: GSI Helmholtzzentrum für Schwerionenforschung GmbH, Planckstraße 1, 64291 Darmstadt, Germany

ABSTRACT

Direct laser acceleration (DLA) of electrons in a plasma of near-critical electron density (NCD) and the associated synchrotron-like radiation are discussed for moderate relativistic laser intensity (normalized laser amplitude $a_0 \le 4.3$) and ps length pulse. This regime is typical of kJ PW-class laser facilities designed for high-energy-density (HED) research. In experiments at the PHELIX facility, it has been demonstrated that interaction of a 10^{19} W/cm^2 sub-ps laser pulse with a sub-mm length NCD plasma results in the generation of high-current well-directed super-ponderomotive electrons with an effective temperature ten times higher than the ponderomotive potential [Rosmej *et al.*, Plasma Phys. Controlled Fusion **62**, 115024 (2020)]. Three-dimensional particle-in-cell simulations provide good agreement with the measured electron energy distribution and are used in the current work to study synchrotron radiation from the DLA-accelerated electrons. The resulting x-ray spectrum with a critical energy of 5 keV reveals an ultrahigh photon number of 7×10^{11} in the 1–30 keV photon energy range at the focused laser energy of 20 J. Numerical simulations of betatron x-ray phase contrast imaging based on the DLA process for the parameters of a PHELIX laser are presented. The results are of interest for applications in HED experiments, which require a ps x-ray pulse and a high photon flux.

I. INTRODUCTION

Synchrotron-like radiation generated by electrons during laser-plasma acceleration is characterized by a broadband x-ray spectrum with a small divergence and a high brilliance. It provides an excellent tool for hard x-ray radiography and x-ray phase contrast high-resolution imaging in biology[1–3] and medicine[4] and in investigations of ultra-fast processes in laser-driven shock waves[5,6] or implosions.[7,8] A detailed overview of the applications of betatron radiation is given in Ref. 9. The characteristics of betatron radiation, such as the critical energy E_c, photon number, bandwidth, source size,

and divergence angle, depend on the mechanism of electron acceleration, the electron energy distribution, and the charge carried by electrons.

Extensive experimental studies of synchrotron radiation were performed at sub-100 fs pulse laser systems in the laser wakefield acceleration (LWFA) regime of electron acceleration,[10–12] where the production of quasi-mono-energetic GeV electron beams was demonstrated[13,14] in an underdense plasma with an electron density of ~10^{18} cm^{-3}. Electrons confined in the focusing phase of the plasma wake experience transverse betatron oscillations, emitting highly collimated synchrotron x-rays. In such experiments, the charge carried by electrons is far below the nC level, and the number of photons around the critical energy E_c of some keV does not exceed 10^9. Nevertheless, a short pulse duration and low divergence angle resulted in a record brilliance of 10^{23} photons s^{-1} mm^{-2} $mrad^{-2}$ $(0.1\%\ BW)^{-1}$ (where BW is the bandwidth).[12]

Increases in the plasma density and/or laser pulse duration at relativistic laser intensity can lead to longitudinal breakup ("self-modulation") of the laser pulse.[15,16] For the self-modulated regime of acceleration (SMLWFA), the laser pulse must be substantially longer than the period of electron Langmuir electron oscillations. As a result, the wake takes a form of a rapidly evolving train of electron cavities driven by relativistic intense optical bullets. This turns the electron spectrum into a quasi-Maxwellian one, while increasing the accelerated charge by more than one order of magnitude compared with the LWFA case. Measurements of the betatron radiation generated in the self-modulated LWFA regime at the sub-ps sub-kJ Titan laser system were reported in Refs. 17 and 18. Up to 10^9 photons eV^{-1} sr^{-1} at 6 keV were measured in the interaction of a 150 J laser pulse with an underdense plasma of $\leq 10^{19}$ cm^{-3} electron density. Simulations performed for the 1.1 kJ sub-ps PETAL conditions[8] showed that the SMLWFA regime predicts up to 10^{12} emitted photons in the energy range of 2–60 keV and a high brilliance of 5×10^{20} photons s^{-1} mm^{-2} $mrad^{-2}$ $(0.1\%\ BW)^{-1}$.

Simulations of synchrotron radiation generated in a near-critical electron density (NCD) plasma by direct laser-accelerated electrons were performed for ultrarelativistic laser intensities $\geq 10^{21}$ W/cm^2 and fs-short laser pulses.[19,20] These simulations demonstrated the generation of $\geq 10^{10}$ MeV photons in 0.1% BW with a critical energy of 5 MeV as a result of electron acceleration up to 1 GeV energy and high transverse focusing force at a high plasma density of $n_e = 1.8\ n_{cr}$.[20] [The critical electron density is defined as $n_{cr} = m_e\omega_L^2/(4\pi e^2)$, where m_e and e are the electron rest mass and electron charge and ω_L is the laser frequency.]

In this work, we explore synchrotron radiation in a long-scale NCD plasma at moderate relativistic laser intensity, for parameters typical of kJ PW-class laser facilities currently in operation, and demonstrate the feasibility of a direct laser acceleration (DLA)-based betatron source that promises an ultrahigh number of x-ray photons for applications in high-energy-density (HED) research. The use of low-density foams has paved the way to the practical realization of DLA in NCD plasmas and has demonstrated its high robustness.

In pilot experiments performed on the Petawatt High Energy Laser for Ion Experiments (PHELIX) facility at the GSI Helmholtzzentrum Darmstadt,[21,22] a long-scale NCD plasma with a thickness of 300–500 μm and an electron density of $\leq 10^{21}$ cm^{-3} was produced using a well-controlled ns pulse that triggered a supersonic ionization wave[23] in a low-density polymer aerogel.[24] Accelerated electrons with an effective temperature of 10–20 MeV and electron energies up to 100 MeV carry up to μC charge.[21,22] 3D particle-in-cell (PIC) simulations performed for the PHELIX laser intensity of 2.5×10^{19} W/cm^2 and 20 J contained in the full width at half maximum (FWHM) of the focal spot predict synchrotron radiation with 7×10^{11} photons (1–30 keV) and a critical energy $E_c \simeq 5$ keV.

The remainder of the paper is organized as follows. In Sec. II, experimental data[22] that demonstrate realization of the DLA process in sub-mm long pre-ionized polymer foams are presented. In Sec. III, the parameters of the betatron radiation obtained from 3D PIC simulations based on the experimental results obtained on the PHELIX facility are discussed. The DLA-based betatron source is compared with synchrotron radiation generated in the LWFA and SMLWFA regimes at different laser systems. Section IV presents simulations of x-ray phase contrast imaging (XPCI) using the calculated DLA-based betatron source for radiographic applications in HED experiments. Section V summarizes the results.

II. DLA IN PLASMA OF NEAR-CRITICAL DENSITY

The electron acceleration in relativistic laser channels generated by intense laser pulse in an NCD plasma was discussed for the first time in Refs. 25 and 26, where a mechanism of direct laser energy coupling into hot electrons was proposed that requires strong self-generated static electric and magnetic fields (Fig. 1). A relativistic laser pulse propagating in an NCD plasma experiences strong self-focusing. Ponderomotive expulsion of background plasma electrons from the plasma channel creates a radial electrostatic field E_r that has a pinching polarity for electrons. At the same time, the current of accelerated electrons generates a strong (≥100 MG)[21,23] azimuthal magnetic field B_ϕ that traps electrons in the ion channel. The betatron radiation is generated when the relativistic electrons undergo transverse betatron oscillations in these self-generated quasistatic fields. An efficient electron energy gain occurs when the betatron frequency becomes close to the Doppler-shifted laser frequency.[25,26]

The DLA works efficiently in plasmas of near critical density (NCD) and in the case of sub-ps laser pulses. To explore this acceleration mechanism, pilot experiments[21,22] were performed on PHELIX.[28] An s-polarized laser pulse of 1.053 μm fundamental wavelength and energy $E_{las} \simeq$ 80–100 J delivered by the Nd:glass laser was focused into an elliptical focal spot with FWHM diameters (12 ± 2) μm and (18 ± 2) μm

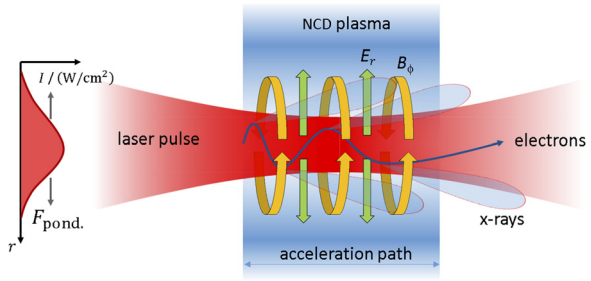

FIG. 1. Betatron radiation is generated when relativistic electrons undergo transverse betatron oscillations in self-generated quasistatic electric and magnetic fields.

using a 150 cm off-axis parabolic mirror. The laser energy in the FWHM of the focal spot was $E_{FWHM} \simeq (17–22)$ J.[22] The peak laser intensity reached $(1–2.5) \times 10^{19}$ W/cm^2 ($a_0 = 2.7–4.28$) at 750 ± 250 fs laser pulse duration. Here a_0 is the normalized vector potential, which scales as $a_0^2 = 0.73 I_{L,18} \lambda^2$, with the laser intensity $I_{L,18}$ normalized to 10^{18} W/cm^2 and the laser wavelength λ in μm. Triacetate cellulose layers of volume density 2 mg/cm^3 and thickness 300–400 μm[26] were used as targets. A sub-mm long NCD plasma was produced by sending a well-defined ns pulse preceding the relativistic main pulse onto foam. The intensity of the ns laser pulse was kept at ~5 × 10^{13} W/cm level to initiate a supersonic ionization wave propagating with 2 × 10^7 cm/s velocity; for more details, see Refs. 21 and 23.

In the experiment,[22] electron spectra were measured in one shot by means of 0.99 T static magnets and imaging plates (IPs) used as detectors. Spectrometers were placed at 0°, 15°, and 45° to the laser axis in the plane perpendicular to the laser polarization at 40 cm from the interaction point. Figure 2(a) presents electron spectra measured by irradiation of a pre-ionized 2 mg/cm^3 CHO foam of 325 μm thickness at ~2 × 10^{19} W/cm^2 laser intensity. The electron energy distributions show a strong angular dependence, with the highest effective temperature and highest electron number close to the laser axis. The electron spectra were approximated by Maxwellian-like distribution functions with one or two temperatures: at 0° with $T = (12.0 \pm 1.4)$ MeV, at 15° with $T_1 \simeq 8.0$ MeV and $T_2 \simeq 11.0$ MeV, and at 45° with $T \simeq 2.9$ MeV. The angular distribution of electrons with energies >3 MeV in a wide range of angles was measured by means of a stack of three stainless steel cylindrical plates.[22] It was shown that super-ponderomotive electrons propagate in a divergence cone of 0.16 sr.

The simulated spectra shown in Fig. 2(b) describe very well the measured electron energy distributions for different angles. The number of simulated super-ponderomotive electrons is up to two to five times higher than measured in the experiment. The experimental number can be corrected upward by at least a factor of two to three owing to the loss of particles by propagation through 20-mm long WCu collimators placed in front of the magnetic spectrometers. It has been suggested that the reason for this effect is a quasistatic electric field created at the collimator front by x-rays or/and high-current relativistic electrons that reached the collimator at the very beginning of the interaction.[29] Electrons that approach the collimator later can be deviated slightly by this field from their initial trajectory and cannot pass through the narrow entrance slit. It can be supposed that this effect is even stronger for electrons detected at 0° to the laser axis, owing to their higher number. This problem will be investigated in more detail in forthcoming experiments.

III. PIC SIMULATIONS OF BETATRON RADIATION

3D PIC simulations of the DLA process in an NCD plasma and the associated synchrotron-like radiation were performed for the laser parameters and interaction geometry described in Ref. 24 using the Virtual Laser Plasma Laboratory (VLPL) code.[30] Laser pulse intensity in time and space was approximated by a Gaussian distribution with an elliptical form of the focal spot taken from the experiment with FWHM axes 11 μm in the vertical and 15 μm in the horizontal direction. The laser pulse energy in the FWHM focal spot of 20 J and the FWHM pulse length of 700 fs resulted in a laser intensity of 2.5×10^{19} W/cm^2 with $a_0 = 4.28$. The homogeneous plasma was composed of electrons and fully ionized ions of carbon, hydrogen and oxygen. Simulations accounted for the ion type and the ion fraction in accordance with the chemical composition of triacetate cellulose, $C_{12}H_{16}O_8$.

Betatron radiation is produced when relativistic electrons undergo transverse betatron oscillations in self-generated magnetic and electrostatic fields. The fundamental dimensionless parameter of betatron radiation is $K = \gamma k_\beta r_\beta$, where γ is the relativistic factor of electrons, and k_β and r_β are respectively the betatron wavenumber and the amplitude of electron betatron oscillations. In the case of $K \gg 1$ (the wiggler regime), the radiation spectrum is quasicontinuous broadband and has a shape given by the universal function $S(\omega/\omega_c)$,[31] where $S(x) = x \int_x^\infty K_{5/3}(\xi) d\xi$, $K_{5/3}$ is a modified Bessel function of the second kind, and $\omega_c = 3K\gamma^2 c k_\beta/2$ is the critical frequency, with c being the speed of light. For frequencies well below the critical

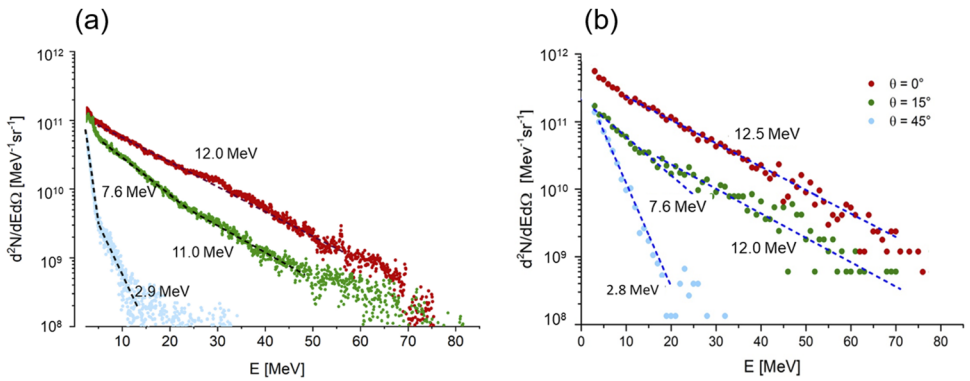

FIG. 2. (a) Energy distribution of super-ponderomotive electrons per steradian measured at 0° (red), 15° (green), and 45° (blue) to the laser propagation direction for a shot onto a pre-ionized foam layer at 2 × 10^{19} W/cm^2 laser intensity. (b) PIC simulations for the same interaction parameters. Reprinted with permission from Rosmej *et al.*, Plasma Phys. Controlled Fusion **62**, 115024 (2020). Copyright 2020 Author(s), licensed under a Creative Commons Attribution 4.0 License.

frequency, the function $S(x)$ increases with frequency as $\omega^{2/3}$, reaches a maximum at ~$0.29\omega_c$, and then drops exponentially to zero above ω_c. For the discussed experimental conditions,[22] the wiggler strength reaches $K \simeq 60$, and the critical photon energy may be expressed as

$$E_c = \hbar\omega_c = \frac{3}{2}\hbar\gamma^3 c r_\beta k_\beta^2. \quad (1)$$

For an electron beam characterized by an effective electron temperature >10 MeV and a charge of ~μC, one expects intense betatron radiation with a large photon number to be generated in the ion channel during the DLA process. In VLPL, at every time step, we assume that the relativistic electrons emit photons in the direction of electron propagation with a spectrum given by $S(\omega/\omega_c)$, where ω_c is determined by $\omega_c = \frac{3}{2}\gamma^2|F_\perp|/(m_e c)$ and $F_\perp$ is the transverse force felt by the electrons.[31,32] The radiation recoil effect is also included in the electron equation of motion. This approach has been widely verified by experiments and independent simulations.[10,12,33,34]

Figure 3(a) shows the spectral distribution of the betatron radiation simulated for the PHELIX laser parameters ($a_0 = 4.28$, 0.7 ps, and $E_{FWHM} = 20$ J) presented in a semi-logarithmic plot. The betatron spectrum peaks at 1.7 keV and has a critical energy of 5 keV. The x-ray photon number reaches 6×10^{11} in the 1–10 keV energy range and 1×10^{11} in the 10–60 keV range. A 0.1% BW at ~5 keV contains ~3×10^8 photons. According to simulations, a laser pulse in an NCD plasma undergoes strong self-focusing, resulting in a 4 μm [root mean square (rms)] transverse radius of the radiation source. Source opening angles at the critical energy in the Y (polarization) and Z directions are rather large, reaching θ_{FWHM}: 840 and 640 mrad, respectively. In spite of the large divergence, the abovementioned characteristics of the DLA-based betatron source ensure a high brilliance $B(\theta_{FWHM}) \simeq 6 \times 10^{19}$ photons s^{-1} mm^{-2} mrad^{-2} (0.1% BW)$^{-1}$.

Figure 3(b) shows a 2D map of the photon fluence at the detector at a distance of 120 cm from the source. The distribution of the radiation is not very homogenous: one can observe two hot spots in the polarization direction that are two to three times more intense than the surrounding area. The photon fluence at the detector remains at a very high level, up to 10^8 x-ray photons/cm^2, which is very promising for applications in HED research.

Table I presents characteristics of betatron sources produced via different mechanisms of electron acceleration, such as LWFA, SMLWFA, and DLA. It shows the parameters of the laser–target interaction and the characteristics of the generated ultrarelativistic electrons and betatron sources. The betatron radiation produced in the LWFA process has an ultrahigh brilliance, owing to the small source size, low divergence, and tens of fs pulse duration.[12] At the same time, only a moderate number of photons is expected, owing to the relatively small charge carried by electrons accelerated in the underdense plasma.

With increasing laser pulse duration and/or plasma density, a transition from LWFA to SMLWFA takes place.[15,16] Experiment[17] and simulations[8] demonstrate an increase in the electron bunch charge up to 10–50 nC and a high x-ray photon fluence. Since the laser pulse undergoes self-focusing by propagation in an underdense plasma, the x-ray source size is smaller than the initial laser focus. Nevertheless, the brilliance suffers owing to a higher x-ray beam divergence and longer pulse duration than in the LWFA case (see Table I).

In the DLA process, μC charge of super-ponderomotive electrons is generated in an NCD plasma.[21,22] An ultrahigh x-ray photon number of ~7×10^{11} is predicted by numerical simulations performed for the laser and target parameters used in the experiment [$E_{las} \simeq 80$ J ($E_{FWHM} \simeq 20$ J), 0.7 ps, $a_0 = 4.2$, and a target consisting of a 300 μm long NCD layer with electron density 6.5×10^{20} cm^{-3}]. This photon number is similar to that obtained for the SWLWFA-based betatron source in simulations performed for the PETAL laser parameters (1.1 kJ, 0.5 ps, and $a_0 = 7$) and a centimeter-long plasma target with electron density (1–3) $\times 10^{18}$ cm^{-3} (see Table I). This can be explained by the higher plasma density in the case of the NCD target and the correspondingly large number of electrons (~1 μC)[21,22] that are involved in the DLA-process and generate betatron radiation.

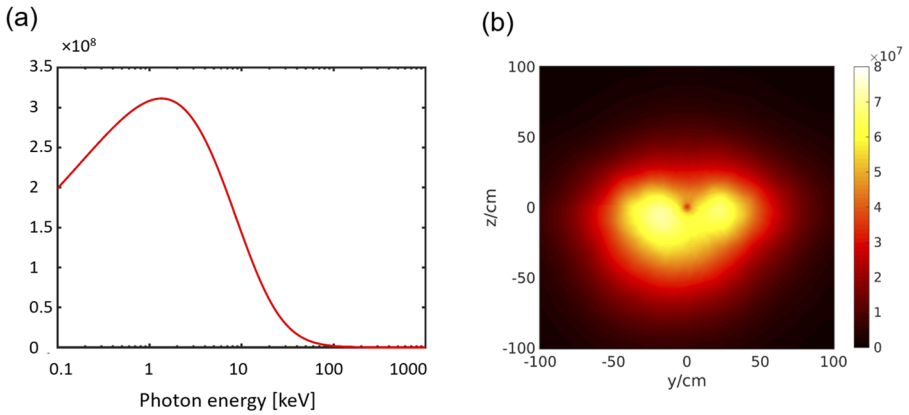

FIG. 3. (a) Spectral distribution of the betatron radiation simulated for the PHELIX parameters. (b) 2D map of the photon fluence at the detector placed at a distance of 120 cm from the source.

TABLE I. Comparison of betatron sources produced in LWFA, SMLWFA, and DLA processes.

Laser/target	Regime	Electrons	X-rays	Brilliance	References
ASTRA-GEMINI 50 fs, 5 J, 35 μm $a_0 \simeq 2$ $N_e \simeq 10^{18}$ cm^{-3}	Resonant betatron oscillations in plasma wake; experiment	$E_{max} \simeq 700$ MeV Q_e N/A	$N_{ph} \simeq 5 \times 10^8$ $E_c \simeq 50$–450 keV $\theta_{FWHM} = 14$ mrad Source size $L_{RMS} \simeq 15$ μm	10^{23}	12
TITAN 0.7 ps, 120 J, 20 μm $a_0 \simeq 3$ $N_e \simeq 10^{19}$ cm^{-3} supersonic gas-jet	SMLWFA; experiment	$T_{hot} \simeq 15$ MeV $E_{max} \simeq 300$ MeV $Q_e \simeq 10$ nC	$N_{ph} \simeq 10^9$ eV^{-1} sr^{-1} $\Delta E_{ph} \simeq 6.5 \pm 0.5$ keV $E_c \simeq 10$ keV $\theta_{FWHM} =$ $L_{RMS} \simeq 35$ μm	N/A	17 and 18
PETAL 0.5 ps, 1 kJ, 42 μm $a_0 \simeq 7.5$ $N_e \simeq (1$–$3) \times 10^{18}$ cm^{-3} cm-long plasma	SMLWFA; CALDER-CIRC simulations	$E_e \simeq 1$ GeV $Q_e \simeq 38$ nC (>70 MeV)	$N_{ph} \simeq 7 \times 10^{11}$ $\Delta E_{ph} \simeq 2$–60 keV $E_c \simeq 10$ keV $\theta_{FWHM} = 50$ mrad $L_{RMS} \simeq 25$ μm	5×10^{20}	8
PHELIX 0.7 ps, 80 J ($E_{FWHM} \simeq 20$–30 J), 15 μm $a_0 \simeq 3$–4 $N_e \simeq 0.6 \times 10^{21}$ cm^{-3} pre-ionized low-density polymer aerogels	DLA at betatron resonance; experiment and 3D PIC	$T_{hot} \simeq 13$ MeV $E_{max} \simeq 100$ MeV $Q_e \simeq 1$ μC (>2 MeV) $Q_e \simeq 100$ nC (>7 MeV) experiment	$N_{ph} \simeq 6 \times 10^{11}$ $\Delta E_{ph} \simeq 1$–10 keV $N_{ph} \simeq 10^{11}$ (>10 keV) $E_c \simeq 5$ keV $\theta_{FWHM} \simeq 700$ mrad $L_{RMS} \simeq 4$ μm 3D PIC	6×10^{19} (θ_{FWHM})	22 Current work

Although the maximum electron energy is lower than that from the SWLWFA scheme, the two orders of magnitude higher background plasma density exerts a much stronger transverse focusing force $F_\perp$ on the relativistic electrons in the plasma channel. Because $\omega_c = \frac{3}{2}\gamma^2|F_\perp|/(m_e c)$,[31,32] the photon critical energy in the DLA case differs by a factor of only two to five from those in LWFA and SMLWFA, despite a significantly lower Lorentz factor γ of the accelerated electrons. The drawback of the high electron density (high focusing force) is an opening angle that is ten times larger than in the SMLWFA case.[8]

When comparing the performance of LWFA- and DLA-driven betatron sources, it is also important to consider the level of parasitic background radiation in experiments where x-ray phase contrast imaging (XPCI) is applied. The LWFA-based betatron radiation provided by sub-100 TW short-pulse lasers, which deliver joules of energy on target, has been used successfully to radiograph biological objects[1–3] demanding a high spatial resolution. A photon number of 10^8–10^9 was sufficient for XPCI in one shot owing to the low background radiation. In HED research,[18,36,37] kJ PW-class lasers produce a high level of parasitic radiation caused by a large amount of accelerated particles and radiation, which interact with the target chamber and diagnostic setup. Under these hazardous conditions, an ultrahigh photon number is required to ensure a high signal-to-noise ratio of the XPCI technique.

Scaling the DLA process toward higher laser energy while keeping the laser pulse duration and focal spot size constant will result in a growth in laser field amplitude and consequent increases in electron energies and the number of DLA electrons. In an NCD plasma at high laser power, the acceleration process can be hindered by the filamentation and hosing instabilities of the laser pulse propagating in the plasma channel. 3D PIC simulations performed for higher laser energy and intensity have demonstrated that in this case, the DLA process continues to be very effective[27,35] and can ensure enhanced production of betatron radiation.

IV. X-RAY PHASE CONTRAST IMAGING SIMULATIONS FOR PHELIX

High-energy PW-class laser systems such as PHELIX are designed for HED research and the study of matter in extreme states. In this context, time-resolved x-ray absorption and XPCI radiography using bremsstrahlung emission was performed on PHELIX to study a laser-driven shock wave traveling in a target material.[36,37] The nanosecond evolution of the shock wave requires an x-ray pulse in the ps regime and a high photon flux to freeze the phenomenon in a single-shot experiment. Bremsstrahlung sources can be very bright, but the isotropic emission can produce a large noise induced by the irradiation of the entire chamber and components. In this sense, betatron radiation represents an improvement because of its directionality. Moreover, this radiation is generated in low-Z polymer foams, whereas bremsstrahlung sources are obtained by irradiating a high-Z target to increase the photon yield. The directionality of the betatron x-ray beam makes it possible to place both object and detector at greater distances from the x-ray source, thereby preserving the photon flux. Increases in the source–object distance R_0 and the object–detector distance R_1 have a beneficial effect on phase

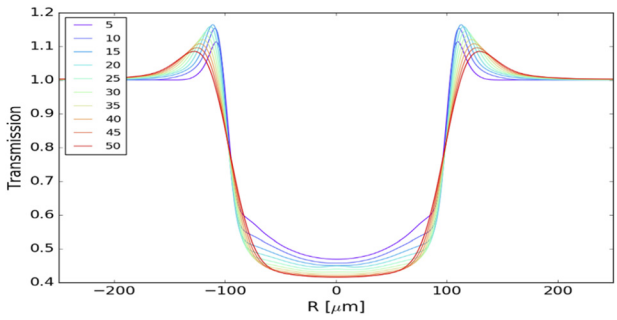

FIG. 4. Comparison of line out for different distances from $R_0 = 5$ to $R_0 = 50$ cm. The total distance $R_0 + R_1 = 120$ cm. The highest phase enhancement was observed at $R_0 = 15$ cm.

enhancement. For a noncoherent source such as a bremsstrahlung or betatron source, it is still possible to define what is called the lateral coherence L_c:

$$L_c = \frac{\lambda R_0}{s}, \tag{2}$$

where s is the source size. The lateral coherence defines the maximum distance between two points on the wave front that are able to interfere and to coincide with the enhancement. L_c increases with increasing distance R_0, while the source size is kept as small as possible. Moreover, the x-ray energy plays a role, because higher energy leads to a smaller value of L_c. However, because of the competition between absorption and phase shift, the constraint on the wavelength for lateral coherence can be compensated with the distance R_0, supporting the contribution of the phase against the absorption. To maximize phase enhancement compared with absorption, the best setup for XPCI has to take into account all the x-ray source parameters.

For the PHELIX parameters discussed here, 3D PIC simulations predict an ultrahigh photon fluence (see Table I) that remains at the level of 10^8 cm^{-2} at 120 cm distance from the target [Fig. 3(b)]. XPCI simulations were performed to predict the imaging performance using the DLA-based betatron radiation predicted by the simulations in Sec. III. The code was designed to calculate x-ray absorption and phase contrast, taking into account the x-ray spectrum, source size, and spatial intensity distribution and solving the Kirchhoff–Fresnel equation using the Fresnel approximation.[38] The code works in a cylindrical geometry and takes into account the detector resolution and the density map associated with the object.

For simulations of the betatron based XPCI-experiment on the PHELIX facility, a sphere of polystyrene (CH) with density $\rho = 1.046$ g/cm^3 and radius $r = 100$ μm was chosen as the test target. Plastic spheres are commonly used for studies of, for example, Rayleigh–Taylor instabilities[39] and strong shocks.[40] Plastic is quite transparent to hard radiation, and this is a key point if one wants to underline the contribution of the phase contrast against the absorption. The betatron source parameters such as x-ray spectrum, source size, and opening angle were taken from the 3D PIC simulations presented in Sec. III. For a total distance $R_0 + R_1 = 120$ cm, where R_0 is the distance between the betatron source and the object and R_1 is that between the object and the detector, a set of simulations were first performed in which the distance R_0 was varied from 5 to 50 cm. The estimated x-ray photon fluence reaches 100 photons 10 μm^2 for the total distance $R_1 + R_0 = 120$ cm. A large distance between the betatron source and the detector, which can be realized owing to ultrahigh photon fluence, allows for a higher spatial coherence, a higher image magnification, and consequently a better spatial resolution. Figure 4 shows a comparison of the line out along the sphere axis for all the distances considered. The contribution of the phase enhancement on the edge of the sphere is clear. The edge intensity increases with distance R_0 up to $R_0 = 15$ cm and then starts to decrease again. This initial set of simulations were performed assuming a single photon energy of 5 keV.

The lateral coherence at the critical energy of 5 keV reaches $L_c = 4$ μm for $R_0 = 15$ cm and a source size $s = 10$ μm. The spatial resolution is limited by the pixel size of the IP. When the magnification of the optimized setup geometry $M = 7$ and the IP resolution of ~100 μm/pixel are taken into account, a spatial resolution of ~15 μm is expected.

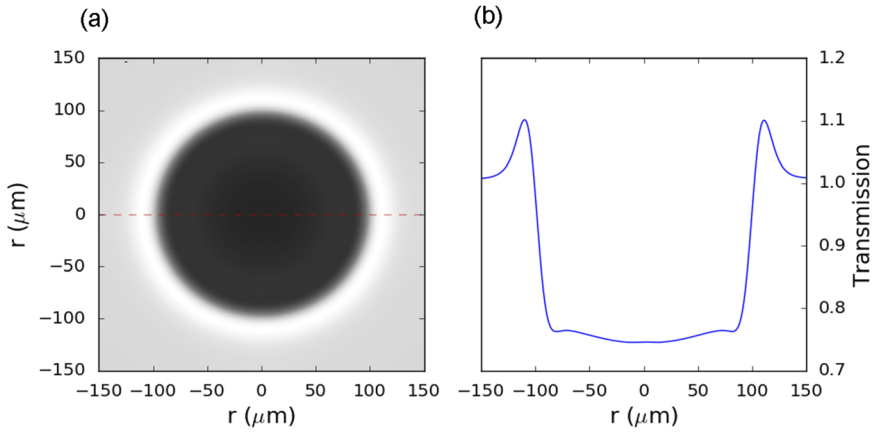

FIG. 5. (a) Simulated XPCI radiograph. (b) Line out along the sphere axis [red dashed line in (a)]. The presence of phase enhancement is clearly visible around the sphere. We considered the betatron emission up to 40 keV and the sensitivity curve of the BAS-TR IP. For the x-ray source size, the worst case was assumed (an initial laser spot size of 15 μm).

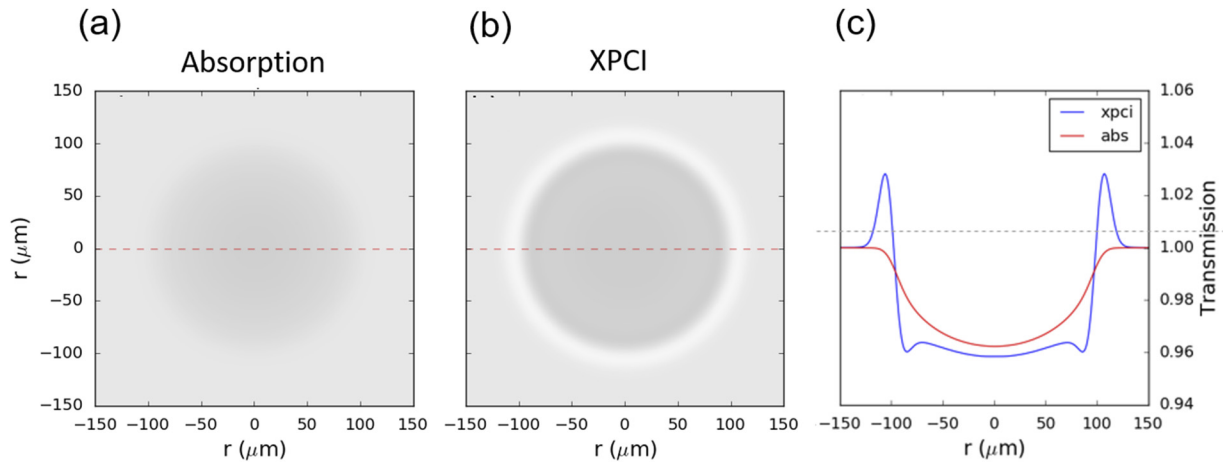

FIG. 6. Comparison between (a) absorption and (b) XPCI. The line out across the cylinder axis in (c) reveals the contribution of phase enhancement to the detection of the sphere, absorption by which is otherwise too weak to allow its detection under standard noisy experimental conditions.

Figure 5 presents a simulated phase contrast image of the sphere in which the whole betatron emission up to 40 keV (see the spectrum in Fig. 3) and the sensitivity curve of the IP (a Fuji BAS-TR plate) were taken into account. The result is shown in Fig. 5(a), and the line out along the sphere axis is shown in Fig. 5(b). The effect of the phase enhancement is clearly visible at the sphere border, where the density exhibits the vacuum–target discontinuity.

To compare XPCI with simple absorption radiography, a sphere with a density ten times lower than the solid CH sphere was irradiated with the simulated betatron spectrum [Fig. 3(a)] in the optimized setup geometry. The resulting absorption image is shown in Fig. 6(a) and the XPCI in Fig. 6(b).

For the considered sphere areal density ($\rho x \leq 100$ mg/cm^3 $\times$ 200 μm) the absorption of photons with energies between 4 and 10 keV is very low (0.04%–0.7%). Therefore, it is difficult to detect the sphere with pure absorption radiography, whereas the presence of the sphere is obvious in the XPCI image owing to the phase enhancement. Furthermore, from the line-out comparison in Fig. 6(c), we can observe the increasing contrast due to the phase contribution.

The comparison between absorption radiography and XPCI shown in Fig. 6 suggests that by using the XPCI technique with high-energy x-ray radiation, it is still possible to detect objects with a low areal density even when the intensity contrast in the absorption image makes absorption radiography ineffective. In the presence of strong density gradients and density interfaces in the object, the contribution of phase enhancement depends weakly on the energy of the x-ray radiation. Simulations show that the lower limit on the volume density for detection of an object with a size of 100–200 μm is 10 mg/cm^3. This important feature means that the requirements on x-ray source properties for XPCI are less restrictive than in the case of standard absorption radiography.

V. CONCLUSION

In this work, the feasibility of a DLA-based betatron source that promises an ultrahigh number of x-ray photons has been demonstrated. Numerical simulations of the intense betatron radiation that occurs in the DLA process and its radiographic applications have been discussed for the present parameters of the PHELIX facility.

The simulations are based on the experimentally confirmed scheme of electron acceleration in an NCD plasma during the interaction of a sub-ps laser pulse (~0.7 ps) at a moderate relativistic laser intensity of ~2×10^{19} W/cm^2 with sub-mm length pre-ionized polymer foams.[22] The use of low-density foams has paved the way to the practical implementation of DLA in NCD plasmas, requiring neither ultrahigh laser intensity nor high laser contrast, and has demonstrated its high robustness.

3D PIC simulations of the interaction of a 0.7 ps, 2×10^{19} W/cm^2 laser pulse with a long-scale NCD plasma reveal the generation of betatron radiation with an ultrahigh photon number of 7×10^{11} per shot in the 1–30 keV range obtained for 20 J focused laser energy. The brilliance of the betatron source reaches $\geq 6 \times 10^{19}$ photons s^{-1} mm^{-2} mrad^{-2} (0.1% BW)$^{-1}$ at the critical energy of 5 keV. It is to be expected that increasing the laser energy while keeping the laser pulse duration and focal spot size constant will lead to a growth in the energy and number of DLA electrons and to a corresponding increase in the betatron critical energy and x-ray photon number. This approach, which promises well-directed ultrahigh-fluence x-ray beams delivered on a ps time scale, will significantly enhance the radiographic capabilities of kJ PW-class laser systems operating in HED research.

ACKNOWLEDGMENTS

The experimental results presented here are based on Experiment P176 performed at the PHELIX facility at the GSI Helmholtzzentrum fuer Schwerionenforschung, Darmstadt (Germany) in the framework of FAIR Phase-0. The experimental group is very grateful for the support provided by the PHELIX laser team at GSI-Darmstadt. This work was also supported by the DFG (Project No. PU 213/9), EPSRC Grant No. EP/P026796/1. The authors gratefully acknowledge the Gauss Centre for Supercomputing e.V. for funding this project by providing computing time on the GCS Supercomputer JUWELS at Jülich Supercomputing Centre (JSC). X.F.S. gratefully acknowledges support by the Alexander von Humboldt Foundation.

The research of V.S.P. and N.E.A. was supported by the Ministry of Science and Higher Education of the Russian Federation (Agreement with Joint Institute for High Temperatures RAS No 075-15-2020-785, dated September 23, 2020).

REFERENCES

[1]S. Fourmaux, S. Corde, K. T. Phuoc *et al.*, "Single shot phase contrast imaging using laser-produced Betatron x-ray beams," Opt. Lett. **36**, 2426 (2011).
[2]S. Kneip, C. McGuffey, F. Dollar *et al.*, "X-ray phase contrast imaging of biological specimens with femtosecond pulses of betatron radiation from a compact laser plasma wakefield accelerator," Appl. Phys. Lett. **99**, 093701 (2011).
[3]J. Wenz, S. Schleede, K. Khrennikov *et al.*, "Quantitative X-ray phase-contrast microtomography from a compact laser-driven betatron source," Nat. Commun. **6**, 7568 (2015).
[4]J. M. Cole, J. C. Wood, N. C. Lopes *et al.*, "Laser-wakefield accelerators as hard x-ray sources for 3D medical imaging of human bone," Sci. Rep. **5**, 13244 (2015).
[5]J. C. Wood, D. J. Chapman, K. Poder *et al.*, "Ultrafast imaging of laser driven shock waves using betatron x-rays from laser wake-field accelerator," Sci. Rep. **8**, 11010 (2018).
[6]A. Ravasio, M. Koenig, S. Le Pape *et al.*, "Hard x-ray radiography for density measurement in shock compressed matter," Phys. Plasmas **15**, 060701 (2008).
[7]J. Lindl, "Development of the indirect-drive approach to inertial confinement fusion and the target physics basis for ignition and gain," Phys. Plasmas **2**, 3933 (1995).
[8]J. Ferri, X. Davoine, S. Y. Kalmykov, and A. Lifschitz, "Electron acceleration and generation of high brilliance x-ray radiation in kilojoule, sub-picosecond laser-plasma interactions," Phys. Rev. Accel. Beams **19**, 10130 (2016).
[9]F. Albert and A. G. R. Thomas, "Applications of laser wakefield accelerator-based light sources," Plasma Phys. Controlled Fusion **58**(10), 103001 (2016).
[10]A. Rousse, K. T. Phuoc, R. Shah *et al.*, "Production of a keV x-ray beam from synchrotron radiation in relativistic laser-plasma interaction," Phys. Rev. Lett. **93**(13), 135005 (2004).
[11]J. Ju, K. Svensson, A. Döpp *et al.*, "Enhancement of x-rays generated by a guided laser wakefield accelerator inside capillary tubes," Appl. Phys. Lett. **100**, 191106 (2012).
[12]S. Cipiccia, M. R. Islam, B. Ersfeld *et al.*, "Gamma-rays from harmonically resonant betatron oscillation in plasma wake," Nat. Phys. **7**, 867 (2011).
[13]V. Malka, "Laser plasma accelerators," Phys. Plasmas **19**, 055501 (2012).
[14]T. Tajima and J. M. Dawson, "Laser electron accelerator," Phys. Rev. Lett. **43**, 267 (1979).
[15]N. E. Andreev, L. M. Gorbunov, V. I. Kirsanov *et al.*, "Resonant excitation of wake-fields by a laser pulse in a plasma," JETP Lett. **55**(3), 571–577 (1992).
[16]N. E. Andreev, V. I. Kirsanov, and L. M. Gorbunov, "Stimulated processes and self-modulation of short intense laser pulses in laser wake field accelerator," Phys. Plasmas **2**(6), 2573–2582 (1995).
[17]F. Albert, N. Lemos, J. L. Shaw *et al.*, "Observation of betatron x-ray radiation in a self-modulated laser wakefield accelerator driven with picosecond laser pulses," Phys. Rev. Lett. **118**(13), 134801 (2017).
[18]F. Albert, N. Lemos, J. L. Shaw *et al.*, "Betatron x-ray radiation in the self-modulated laser wakefield acceleration regime: Prospects for a novel probe at large scale laser facilities," Nucl. Fusion **59**(3), 032003 (2018).
[19]H. Y. Wang, B. Liu, X. Q. Yan, and M. Zepf, "Gamma-ray emission in near critical density plasmas at laser intensities of 10^{21} W/cm^2," Phys. Plasmas **22**, 033102 (2015).
[20]T. W. Huang, A. P. L. Robinson, C. T. Zhou *et al.*, "Characteristics of betatron radiation from direct-laser-accelerated electrons," Phys. Rev. E **93**, 063203 (2016).
[21]O. N. Rosmej, N. E. Andreev, S. Zaehter *et al.*, "Interaction of relativistically intense laser pulses with long-scale near critical plasmas for optimization of laser based sources of MeV electrons and gamma-rays," New J. Phys. **21**, 043044 (2019).
[22]O. N. Rosmej, M. Gyrdymov, M. M. Günther *et al.*, "High-current laser-driven beams of relativistic electrons for high energy density research" Plasma Phys. Controlled Fusion **62**, 115024 (2020).
[23]S. Y. Gus'kov, J. Limpouch, P. Nicolaï, and V. T. Tikhonchuk, "Laser-supported ionization wave in under-dense gases and foams," Phys. Plasmas **18**, 103114 (2011).
[24]N. G. Borisenko, A. M. Khalenkov, V. Kmetik *et al.*, "Plastic aerogel targets and optical transparency of undercritical microheterogeneous plasma," Fusion Sci. Technol. **51**(4), 655–664 (2007).
[25]A. Pukhov, Z.-M. Sheng, and J. Meyer-ter-Vehn, "Particle acceleration in relativistic laser channels," Phys. Plasmas **6**(7), 2847 (1999).
[26]A. Pukhov, "Strong field interaction of laser radiation," Rep. Prog. Phys. **66**, 47–101 (2003).
[27]L. P. Pugachev, N. E. Andreev, P. R. Levashov, and O. N. Rosmej, "Acceleration of electrons under the action of petawatt-class laser pulses onto foam targets," Nucl. Instrum. Methods Phys. Res., Sect. A **829**, 88–93 (2016).
[28]V. Bagnoud, B. Aurand, A. Blazevic *et al.*, "Commissioning and early experiments of the PHELIX facility," Appl. Phys. B **100**, 137–150 (2010).
[29]F. Consoli, R. De Angelis, T. S. Rosinson *et al.*, "Generation of intense quasi-electrostatic fields due to deposition of particles accelerated by petawatt-range-laser-matter interactions," Sci. Rep. **9**, 8551 (2019).
[30]A. Pukhov, "Tree-dimensional electromagnetic relativistic particle-in-cell code VLPL (virtual laser plasma lab)," J. Plasma Phys. **61**, 425–433 (1999).
[31]J. D. Jackson, *Classical Electrodynamics*, 3rd ed. (Wiley, New York, 1998).
[32]S. Kiselev, A. Pukhov, and I. Kostyukov, "X-ray generation in strongly nonlinear plasma waves," Phys. Rev. Lett. **93**, 135004 (2004).
[33]C. P. Ridgers, C. S. Brady, R. Duclous *et al.*, "Dense electron-positron plasmas and ultraintense γ rays from laser-irradiated solids," Phys. Rev. Lett. **108**, 165006 (2012).
[34]X. B. Li, B. Qiao, H. X. Chang *et al.*, "Identifying the quantum radiation reaction by using colliding ultraintense lasers in gases," Phys. Rev. A **98**, 052119 (2018).
[35]L. P. Pugachev and N. E. Andreev, "Characterization of accelerated electrons generated in foams under the action of petawatt lasers," J. Phys.: Conf. Ser. **1147**, 012080 (2019).
[36]L. Antonelli, F. Barbato, D. Mancelli *et al.*, "X-ray phase-contrast imaging for laser-induced shock-waves," Europhys. Lett. **125**, 35002 (2019).
[37]F. Barbato, S. Atzeni, D. Batani *et al.*, "Quantitative phase contrast imaging of a shock-wave with a laser-plasma based X-ray source," Sci. Rep. **9**, 18805 (2019).
[38]J. M. Cowley, *Diffraction Physics* (Elsevier, 1995), Vol. 9, p. 481.
[39]D. A. Martinez, V. A. Smalyuk, J. O. Kane *et al.*, "Evidence for a bubble-competition regime in indirectly driven ablative Rayleigh-Taylor instability experiments on the NIF," Phys. Rev. Lett. **114**, 215004 (2015).
[40]R. Nora, W. Theobald, R. Betti *et al.*, "Gigabar spherical shock generation on the OMEGA laser," Phys. Rev. Lett. **114**, 045001 (2015).